Multimaterial filtering applied to the topology optimization of a permanent magnet synchronous machine

Théodore Cherrière, S Hlioui, François Louf, Luc Laurent

Multimaterial filtering applied to the topology optimization of a permanent magnet synchronous machine

Théodore Cherrière*,[a]
Sami Hlioui[b]
François Louf[c]
Luc Laurent[d]

[a] SATIE laboratory, ENS Paris-Saclay, CNRS, Université Paris-Saclay, 91190 Gif-sur-Yvette, France
[b] SATIE Laboratory, CY Cergy Paris University, CNRS, Paris-Saclay University, 95000 Cergy, France
[c] LMPS - Laboratoire de Mécanique Paris-Saclay, Université Paris-Saclay, CentraleSupélec, ENS Paris-Saclay, CNRS, 91190 Gif-sur-Yvette, France
[d] Laboratoire de Mécanique des Structures et des Systèmes Couplés, EA 3196, Conservatoire national des arts et métiers, F-75003 Paris, France

Abstract

- **Purpose** – This work proposes a general methodology to handle multi-material filtering for density-based topology optimization containing periodic or anti-periodic boundary conditions, which are expected to reduce the simulation time of electrical machines. The optimization of the material distribution in a permanent magnet synchronous machine rotor illustrates the relevance of this approach.
- **Design/methodology/approach** – The optimization algorithm relies on an augmented Lagrangian with a projected gradient descent. The 2D finite element method computes the physical and adjoint states to evaluate the objective function and its sensitivities. Concerning regularization, a mathematical development leads to a multi-material convolution filtering methodology that is consistent with the boundary conditions and helps eliminate artifacts.
- **Findings** – The method behaves as expected and shows the superiority of multi-material topology optimization over bi-material topology optimization for the chosen test case. Unlike the standard approach that uses a cropped convolution kernel, the proposed methodology does not artificially reflect the limits of the simulation domain in the optimized material distribution.
- **Originality/value** – Although filtering is a standard tool in topology optimization, no attention has previously been paid to the influence of periodic or anti-periodic boundary conditions when dealing with different natures of materials. The comparison between the bi-material and multi-material topology optimization of a permanent magnet machine rotor without symmetry constraints constitutes another originality of this work.

Keywords: Boundary Conditions – Electrical Machine – Filtering – Non-linear Magnetostatics – Multi-Material Topology Optimization

- Doi: https://doi.org/10.1108/COMPEL-10-2023-0546

Théodore Cherrière, Sami Hlioui, François Louf, , Luc Laurent. Multimaterial filtering applied to the topology optimization of a permanent magnet synchronous machine. COMPEL - The international journal for computation and mathematics in electrical and electronic engineering, *43(4), pp. 852-870, 2024.*
doi: 10.1108/COMPEL-10-2023-0546, hal: hal-04634402

Contents

1 Introduction

Topology optimization (TO) is a set of methods that automatically design technical objects without parameterizing an existing geometry. Since the seminal work of Bendsøe and Kikuchi, 1988 that focuses on homogenization, many different sensitivity-based approaches have been proposed, such as the popular density methods (Bendsøe, 1989), evolutionary strategies (Xie and Steven, 1993), phase-field approach (Wang and Zhou, 2004), or the level-set method, based either on shape (Allaire, Jouve, and Toader, 2004) or on topological derivatives (Amstutz and Andrä, 2006). Driven by the development of additive manufacturing during the last decade (Liu et al., 2018), TO has become mature enough to handle large-scale problems with more than a billion variables (Aage et al., 2017), as well as coupled physics (Feppon et al., 2021) and several different materials (Bruyneel, 2011). In the field of electromagnetic actuators, Dyck and Lowther, 1996 first applied a density method on a magnetic bearing, which was further extended to rotors of electrical machines, including synchronous reluctant machines (J. Lee, Seo, and Kikuchi, 2010); see Lucchini et al., 2022 for a recent overview. The optimization of the rotors of Permanent Magnet Synchronous Machines (PMSM), as in (C. Lee and Gwun, 2022), or their stators (Cherrière, Laurent, et al., 2022), involve Multi-Material Topology Optimization (MMTO) that density-based approaches can handle. The main idea is to extend the dimension of the interpolation domain by considering vector density fields that encode the intermediate materials. The interpolation can be constructed either with a product-based approach (Sigmund, 2001) or by using shape functions on a hypercube (Bruyneel, 2011) that associates each vertex of the interpolation domain with a candidate material. The advantage of hypercube domains is that the projection of the optimization variables onto them is trivial. However, this class of domains is restrictive and does not suit all problems, such as multiphased stator optimization. To overcome this limitation, interpolation domains can be further extended to all convex polytopes denoted as $\mathscr{D}$ (Cherrière, Laurent, et al., 2022) in which each position interpolates the material properties between candidate materials located at its vertices. The density-based optimization problem on a design domain Ω_d then reads

$$\text{find} \quad \boldsymbol{\rho}_{\text{opt}} = \arg \min_{\boldsymbol{\rho}:\Omega_d \to \mathscr{D}} f(\boldsymbol{\rho}). \tag{1}$$

Théodore Cherrière, Sami Hlioui, François Louf, , Luc Laurent. Multimaterial filtering applied to the topology optimization of a permanent magnet synchronous machine. COMPEL - The international journal for computation and mathematics in electrical and electronic engineering, *43(4), pp. 852-870, 2024.*
doi: 10.1108/COMPEL-10-2023-0546, hal: hal-04634402

The optimal solution of (1) may contain intermediate "gray" materials that are located inside $\mathscr{D}$ and not at its vertices, which are associated with proper materials. A solution to eliminate the intermediate materials is the penalization of the material interpolation, which makes the optimization problems non-convex (Abdelhamid and Czekanski, 2022) and leads to "noisy" results that are local optima. Moreover, other numerical artifacts such as checkerboards (Sigmund and Petersson, 1998) are commonly encountered, so density methods are generally paired with a regularization procedure. One of the most standard is density filtering, which solves the Helmholtz equation (Lazarov and Sigmund, 2010), or uses convolution filters (Bourdin, 2001). These methodologies have been frequently used in the case of single materials. In the case of periodic boundary conditions (PBC) or anti-periodic boundary conditions (APBC), the convolution kernel can be extended on the opposite side of the design domain Ω_d by wrapping, as illustrated in Figure 1. In the case of single and bi-material problems, this technique has been applied in mechanical engineering to rectangular design domains regularly meshed (Clausen and Andreassen, 2017; Wallin et al., 2020) and extended to irregular meshes by Kumar and Fernández, 2021.

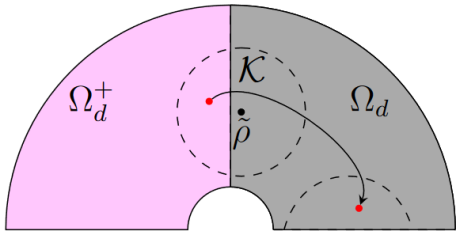

Figure 1: Illustration of a wrapped kernel (Source: Authors' own work).

In the multi-material case, however, an additional difficulty is that the materials' nature may change through the boundary Ω_d, affecting polarized magnetic materials and electrical conductors. In the field of electrical machines, this difficulty is not addressed in the literature to the best of our knowledge. Among the work dealing with topology optimization of rotor poles, filtering schemes are nevertheless applied, without being detailed. Symmetry with respect to the d axis is generally imposed (C. Lee and Gwun, 2022; Korman et al., 2022). In this case, the material continuity through the (anti-)periodic boundaries can not be satisfied (except in special cases when the magnetization is orthogonal to the boundary). However, symmetry constitutes an unnecessary restriction, since optimized designs can present natural asymmetry as shown by Cherrière, Hlioui, Laurent, Louf, Ben Ahmed, et al., 2022; Gauthey, Hassan, et al., 2024. When symmetry is not imposed, the boundary conditions are either not discussed (Cherrière, Vancorsellis, et al., 2023), or the entire machine is simulated (Gauthey, Gangl, and Hage Hassan, 2022), leading to low resolution to keep an acceptable computing time. Recently, Cherrière, Hlioui, Laurent, Louf, Ahmed, et al., 2024 includes the anti-periodic boundary condition consideration in the case of stator optimization, considering only iron and conductors.

Considering any material, this work proposes a rigorous and systematic extension to apply convolution filtering to MMTO with (anti-) periodic boundary conditions in a magnetostatic or any other physical context. First, Section 2 recalls the MMTO framework. Then, Section 3 explains mathematically the different steps of boundary management in the filtering process. Section 4 applies the methodology to optimize a PMSM rotor and compares it with alternative approaches. Finally, Section 5 synthesizes the main results and draws some possible prospects from this work.

2 Multi-material topology optimization framework

2.1 Extended density-based approach

Let us consider the following 2D magnetostatics problem (Cherrière, Vancorsellis, et al., 2023) on a simulation domain Ω, which contains a design domain Ω_d:

$$-\nabla\cdot(\nu\nabla a) = \mu_0 j + \nabla\cdot\big(m_y(\boldsymbol{b}) - m_x(\boldsymbol{b})\big), \tag{2}$$

where z is the out-of-the plane axis, a the z component of the magnetic vector potential, j is the z component of the current density, $\boldsymbol{m} = \begin{bmatrix} m_x & m_y & 0 \end{bmatrix}$ the magnetic polarization, and $\boldsymbol{b} = \begin{bmatrix} \mathrm{d}_y a & -\mathrm{d}_x a & 0 \end{bmatrix}$ is the flux density.

The principle of density-based approaches is to interpolate the material properties of (2) between the different candidate materials with a so-called density field $\rho \in \mathscr{L}^\infty(\Omega_d)$ (Cherrière, Laurent, et al., 2022). When dealing with $M > 2$ materials, the density can be extended as a vector field $\boldsymbol{\rho} : \Omega_d \to \mathscr{D} \subset \mathbb{R}^n$, where $\mathscr{D}$ is a convex polytope with n_m vertices, such that each candidate material i is associated with the coordinate $\boldsymbol{v}_i$ of the i-vertex of $\mathscr{D}$. In this formalism, the physical properties of the candidate material i are matched when $\boldsymbol{\rho} = \boldsymbol{v}_i$, and intermediate density values describe fictive isotropic mixtures of the candidate materials. The interpolations of the material properties can be constructed from a set of shape functions $\{\omega_i : \mathscr{D} \to [0,1]\}_{i \in [\![1,n_m]\!]}$ that are identified as generalized barycentric coordinates of $\mathscr{D}$ (Warren et al., 2006). Such functions also satisfy:

$$\text{Lagrange property:} \quad \forall (i,j) \in [\![1,n_m]\!]^2, \;\; \omega_i(\boldsymbol{v}_j) = \delta_{ij}, \tag{3a}$$

$$\text{Linear precision:} \quad \forall \boldsymbol{\rho} \in \mathscr{D}, \;\; \sum_{i=1}^{n_m} \omega_i(\boldsymbol{\rho}) \boldsymbol{v}_i = \boldsymbol{\rho}. \tag{3b}$$

This paper uses the shape functions proposed by Wachspress, 1975, computed with the code provided by Cherrière and Laurent, 2022. Figure 2a shows the interpolation domain used for the PMSM rotor optimization problem, and Figure 2b draws a shape function associated with a 180° magnet orientation.

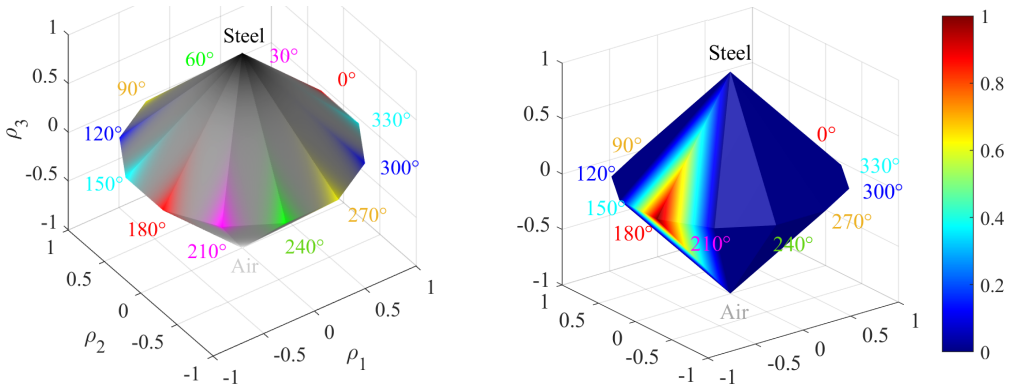

(a) Color-scaled interpolation domain

(b) Values of a shape function

Figure 2: Example of a 3D interpolation domain $\mathscr{D}$ with a shape function for a MMTO problem containing 12 different magnet directions, steel, and air (Source: Authors' own work).

It is also common in TO to penalize the material interpolations in order to eliminate intermediate materials (Bendsøe and Sigmund, 1999), using penalization functions $P_m : [0,1] \to [0,1]$. In this paper, we use a rational penalization scheme proposed by Stolpe and Svanberg, 2001:

$$P_m : \left\{ \begin{array}{ccc} [0,1] & \to & [0,1] \\ \omega & \mapsto & \dfrac{\omega}{1 + p_m(1-\omega)}, \end{array} \right. \tag{4}$$

with p_m a variable coefficient that will be detailed later. Since $j = 0$ in Ω_d, the only interpolation concerns the magnetic polarization:

$$\boldsymbol{m} : \left\{ \begin{array}{ccc} \mathscr{D} \times \mathbb{R}^2 & \to & \mathbb{R}^2 \\ \boldsymbol{\rho}, \boldsymbol{b} & \mapsto & \displaystyle\sum_{i=1}^{M} P_m\big(\omega_i(\boldsymbol{\rho})\big)\, \boldsymbol{m}_i(\boldsymbol{b}), \end{array} \right. \tag{5}$$

that is then injected into (2). After discretization on a mesh with 12443 nodes and 24327 elements using the finite element method, one obtains the non-linear magnetostatic system:

$$\mathbf{K} \cdot \boldsymbol{a}_h = \mathbf{s}\left(j, \boldsymbol{m}(\boldsymbol{\rho}_h, \boldsymbol{b}_h)\right), \tag{6}$$

where $\mathbf{K}$ is the so-called "stiffness" matrix, $\mathbf{a}_h$ is the vector of degrees of freedom, $\mathbf{s}$ is the right-hand side, which depends on the discretized density field $\boldsymbol{\rho}_h$ and the flux density $\mathbf{b}_h$ through (5).

2.2 Optimization problem

The objective is to maximize the average torque $\langle T \rangle$ computed on 121 angular positions with the Arkkio, 1987 method. To obtain meaningful optimized designs, the Permanent Magnets (PM) volume should be limited to an imposed value V_m, otherwise PMs occupy the full rotor. Other constraints, such as torque ripple, mechanical strength, or manufacturability, are possible but omitted for simplicity.The optimization can be conducted by adjusting the density vector $\boldsymbol{\rho}^{\mathscr{T}} \subset \boldsymbol{\rho}_h$ on each element $\mathscr{T}$, so that the PMSM optimization problem reads under the standard form

$$\begin{aligned} \min \quad & f(\boldsymbol{\rho_h}) = -\big\langle\, T\left(\mathbf{a}_h(\boldsymbol{\rho_h})\right) \,\big\rangle, \\ \text{s.t.:} \quad & \text{(i)} \quad \boldsymbol{\rho}^{\mathscr{T}} \in \mathscr{D} \;\;,\;\; \mathscr{T} = 1,...,N, \\ & \text{(ii)} \quad \mathbf{K}\cdot\boldsymbol{a}_h - \mathbf{s}\left(\boldsymbol{m}(\boldsymbol{\rho}_h,\, \mathbf{b}_h), j(\boldsymbol{\rho}_h)\right) = 0, \\ & \text{(iii)} \quad g(\boldsymbol{\rho}_h) = \frac{1}{|\Omega_d|}\int_{\Omega_d} \sum_{i\in I_m} \omega_i(\boldsymbol{\rho}_h) - V_m = 0, \end{aligned} \tag{7}$$

with N the number of mesh elements in Ω_d, I_m the set of indices related to PM vertices, V_m the imposed PM proportion relative to the volume of the optimization zone $|\Omega_d|$. This optimization problem includes three different constraints: (i) is related to the definition domain of the optimization variables; (ii) ensures the physical consistency of the problem; (iii) imposes the PM volume.

2.3 Optimization algorithm

A gradient-based optimization is adopted to solve (7). To handle the global constraint (iii), a classical approach is to define the following augmented Lagrangian function (Nocedal and Wright, 2006):

$$\mathscr{L}(\boldsymbol{\rho}_h, \lambda) = f(\boldsymbol{a}_h(\boldsymbol{\rho}_h)) + \lambda g(\boldsymbol{\rho}_h) + \frac{\mu}{2} g^2(\boldsymbol{\rho}_h), \tag{8}$$

where f is the objective function, g is the constraint (iii), λ is the associated Lagrange multiplier initially set to 0, and $\mu = 10^4$ is a penalization coefficient, so that (7) is solved by finding

$$(\boldsymbol{\rho}_h, \lambda) = \max_{\lambda\in\mathbb{R}} \min_{\boldsymbol{\rho}_h\in\mathscr{D}^N} \mathscr{L}(\boldsymbol{\rho}_h, \lambda), \tag{9}$$

i.e., by solving a sequence of unconstrained subproblems $\min_{\boldsymbol{\rho}_h\in\mathscr{D}^N} \mathscr{L}(\boldsymbol{\rho}_h, \lambda)$ in which λ is fixed. Within this subproblem, a Projected Gradient Descent (PGD) detailed in Cherrière, Laurent, et al., 2022 handles the constraint (i). The constraint (ii) is naturally imposed by using the Adjoint Variable Method (AVM, Cea, 1986), which is an efficient method to compute $\mathrm{d}_{\boldsymbol{\rho}_h} f$ satisfying (ii). In parallel with $\boldsymbol{\rho}_h$, which constitutes the main optimization variables, the phase shift ψ of the current feeding is also controlled to avoid local optima as in Cherrière, Hlioui, Laurent, Louf, Ahmed, et al., 2024. The initial ψ is set to 0°; changing this value leads to a rotation of the optimized rotor with few changes in the overall geometry. The subproblem is solved on sub-cycles of 50 iterations, illustrated in Figure 3, at the end of which λ is updated following

$$\lambda \leftarrow \lambda + \mu g(\boldsymbol{\rho}_h). \tag{10}$$

To eliminate intermediate materials, the penalization factor p_m used in (4) increases gradually from 0 to 4 every 10 iterations and is reset to 0 at the beginning of a new sub-cycle. These values are a trade-off between the computation time and the stability of the algorithm: the longer a sub-cycle is, the better it converges. Note that the design obtained at the end of a sub-cycle constitutes the initial situation of the next one.

Concerning the regularization, the density vector is filtered twice per sub-cycle, which is enough to remove the artifacts. This value is also a compromise between too many filterings leading to blurry boundaries and disturbing the convergence, and not enough that does not remove artifacts efficiently. Note that filtering associated with a high penalization value $p_m > 2$ may lead to instability. The detailed progress of a subproblem is given in Figure 3, and the global optimization algorithm is summarized in Figure 4.

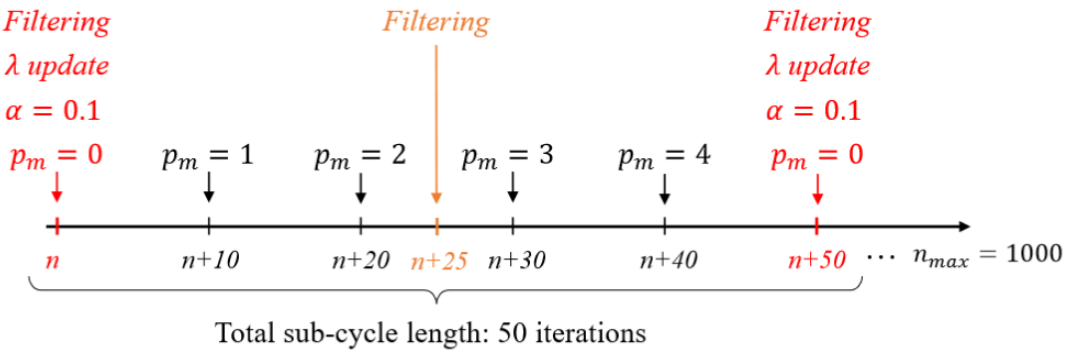

Figure 3: Details of an optimization sub-cycle (Source: Authors' own work).

The convolution filtering should be consistent with the boundary conditions and is detailed in the next section.

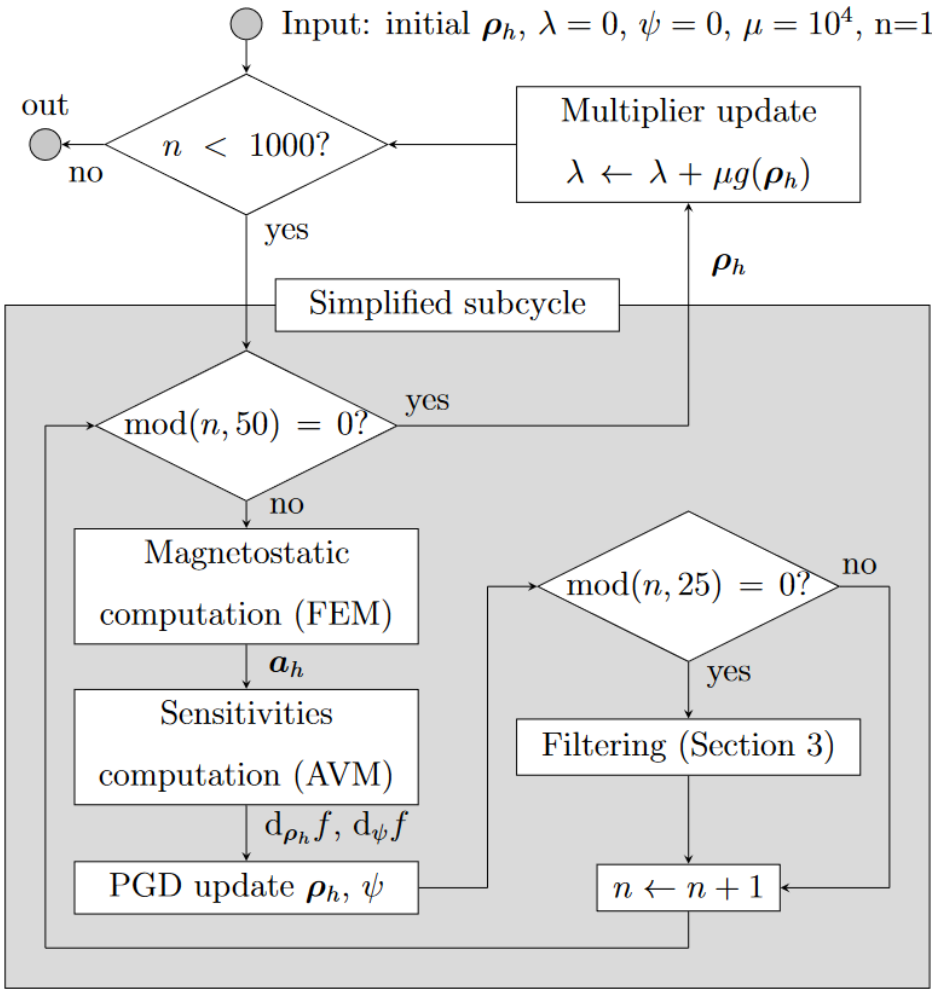

Figure 4: Simplified flowchart of the global optimization algorithm. For the sake of clarity, the update of p_m is not represented; see Figure 3 for the detailed subproblem progress (Source: Authors' own work).

Théodore Cherrière, Sami Hlioui, François Louf, , Luc Laurent. Multimaterial filtering applied to the topology optimization of a permanent magnet synchronous machine. COMPEL - The international journal for computation and mathematics in electrical and electronic engineering, *43(4), pp. 852-870, 2024.*
doi: 10.1108/COMPEL-10-2023-0546, hal: hal-04634402

3 Multi-material filtering

This section details the mathematical considerations to apply multi-material filtering consistent with periodic or anti-periodic boundary conditions. This formalism is not specific to the problem (7), and can be applied as well in other fields where (anti)periodic boundary conditions are required.

3.1 Issues of (anti-)periodic boundary conditions

Convolution filtering is often used in TO to introduce a minimal length scale, which eliminates unwanted numerical artifacts (checkerboard patterns) and noisy local optima, as well as ensures the mesh independence of the optimized results (Sigmund and Petersson, 1998). The principle is to smooth the density field by associating the mesh element $\mathscr{T}$ with the average density of its neighborhood (the kernel), denoted as $\mathscr{K}^{\mathscr{T}}$:

$$\tilde{\boldsymbol{\rho}}^{\mathscr{T}} = \frac{1}{|\mathscr{K}^{\mathscr{T}}|} \int_{\mathscr{K}^{\mathscr{T}}} \boldsymbol{\rho} \, \mathrm{d}\omega. \tag{11}$$

When Ω_d contains PBC or APBC, the kernel should be extended through one side of Ω_d to its opposite side, as illustrated in Figure 5.

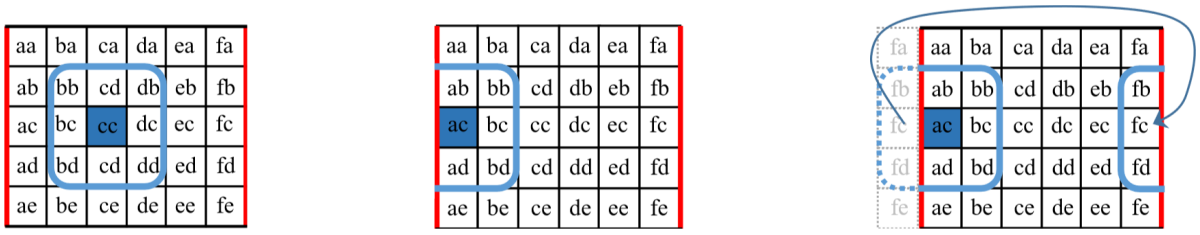

(a) Standard convolution (b) Cropped kernel (c) Wrapped kernel

Figure 5: Illustration of convolution kernel. Red denotes periodic boundaries (Source: Authors' own work).

However, the material properties in the extended kernel might differ from those on the opposite side of Ω_d, leading to a transformation of the associated density field. The following subsections describe this transformation and provide some examples. For the sake of conciseness, only the APBC case is addressed, the extension to PBC being straightforward.

3.2 Transformations of physical fields

APBC are useful for simulating only a single pole of an electrical machine. Therefore, the design domain Ω_d is part of an entire disk $\overline{\Omega_d}$ with an angular opening $\theta_{\max}$ that contains physical fields, *e.g.* the flux density $\boldsymbol{b}$.

Definition 3.1 (Physical field extension)**.** *The extension of a physical field u defined on Ω_d to $\overline{\Omega_d}$ is a linear application that reads for all cylindrical coordinates (r,θ) in $\overline{\Omega_d}$, as:*

$$\begin{aligned} \hat{u}(r,\theta) &= (-1)^{n_\theta} u(r,\theta-\tau\theta_{\max}) && \text{if } u \text{ is scalar,} \\ \hat{\boldsymbol{u}}(r,\theta) &= (-1)^{n_\theta} R(\tau\theta_{\max})\boldsymbol{u}(r,\theta-\tau\theta_{\max}) && \text{if } \boldsymbol{u} \text{ is vector,} \end{aligned} \tag{12}$$

where $\tau = \lfloor \theta/\theta_{\max} \rfloor$ is the floor value of $\theta/\theta_{\max}$ and $R(\theta)$ the rotation matrix by an angle θ.

Such extensions described are illustrated on the upper and lower adjacent domains Ω_d^+ and Ω_d^- in Figure 6.

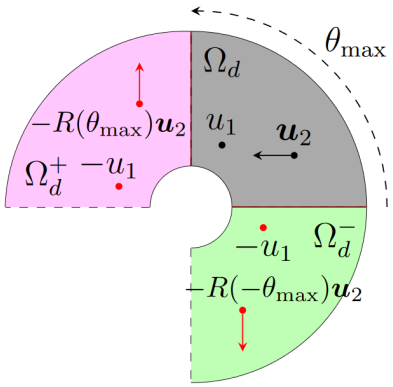

Figure 6: Extension of physical fields in adjacent domains with APBC (Source: Authors' own work).

We now assume that the radius of the convolution kernel is small enough so that we can restrict ourselves to Ω_d, Ω_d^+ and Ω_d^-, without considering the full domain $\overline{\Omega}_d$.

Definition 3.2 (Physical field transformations)**.** *For all physical field u defined on Ω_d, we note*

$$u^+ : (r,\theta) \mapsto \hat{u}(r,\theta+\theta_{\max}) \quad \textit{the corresponding field in } \Omega_d^+, \tag{13a}$$
$$u^- : (r,\theta) \mapsto \hat{u}(r,\theta-\theta_{\max}) \quad \textit{the corresponding field in } \Omega_d^-. \tag{13b}$$

The transformations $\square^+$ and $\square^-$ are linear, norm preserving, and inverse of each other. For the sake of conciseness, we consider only the properties of $\square^+$ in what follows, but the results extend without difficulty to the transformation $\square^-$ by replacing $+$ by $-$ and *vice versa*.

3.3 Transformations of materials

This paragraph aims to define the nature of materials in Ω_d^+ where, compared to Ω_d, all the physical fields have been transformed by $\square^+$.

Definition 3.3 (Material property)**.** *A material property κ is a function that maps a physical field to another:*

$$\kappa : \begin{cases} \mathbb{R}^d & \to \mathbb{R}^d, \quad d = 1 \textit{ or } \dim(\Omega_d), \\ u & \mapsto \kappa(u). \end{cases} \tag{14}$$

Definition 3.4 (Material)**.** *A material $\mathscr{M}$ is an ordered list of n_κ material properties, with κ_k being the k-th of those properties:*

$$\mathscr{M} = (\kappa_k)_{k\in[\![1,n_k]\!]}. \tag{15}$$

We consider a material $\mathscr{M}^+$ obtained from the material $\mathscr{M}$ located in Ω_d, and transformed by $\square^+$ applied to all the physical fields in Ω_d, as illustrated in Figure 6. The transformation of a material property κ could be defined as follows.

Definition 3.5 (Transformation of a material property)**.** *Let us consider κ a material property in the sense of Definition 3.3 and u a physical field. Therefore, we have*

$$\kappa^+ : u \mapsto (\kappa(u^-))^+. \tag{16}$$

The transformations $\square^+$ and $\square^-$ applied to material properties remain linear and inverse of each other. Next, we introduce the *material stability*.

Definition 3.6 (Material stability)**.** *A material is $\square^+$-stable when each of its properties is unchanged by $\square^+$.*

Theorem 3.7 (Stability criteria)**.** *A material is $\square^+$-stable if and only if each of its properties κ_k commutes with $\square^+$, i.e. for all physical field u:*

$$\forall k \in [\![1, n_m]\!], \quad \kappa_k^+ = \kappa_k \quad \Leftrightarrow \quad \kappa_k(u^+) = (\kappa_k(u))^+. \tag{17}$$

Proof. Using Definition 3.5:

- $\boxed{\Rightarrow}$ Assuming $(\kappa(u^+)) = (\kappa(u))^+$, one gets $\kappa^+(u) = (\kappa(u^-))^+ = \kappa((u^-)^+) = \kappa(u)$;
- $\boxed{\Leftarrow}$ Assuming $\kappa^+ = \kappa$, one gets $\kappa(u^+) = \kappa^+(u^+) = (\kappa((u^+)^-))^+ = (\kappa(u))^+$.

■

One can show that $\square^+$ and $\square^-$ stabilities are equivalent, so we refer to the material stability property regardless of the transformation considered. The question is now to determine which materials are stable regarding APBC and which are not. Theorem 3.7 helps discriminate the stable from the unstable materials, as shown in the following examples:

- **Non-polarized magnetic materials are stable**. Indeed, their magnetic polarization $\boldsymbol{m}_b$ is defined with respect to the flux density $\boldsymbol{b}$ as $\boldsymbol{m}_b : \boldsymbol{b} \mapsto \xi(|\boldsymbol{b}|)\boldsymbol{b}$, with ξ a scalar function:

$$\boldsymbol{m}_b(\boldsymbol{b}^+) = \xi(|\boldsymbol{b}^+|)\boldsymbol{b}^+ = (\xi(|\boldsymbol{b}|)\boldsymbol{b})^+ = (\boldsymbol{m}_b(\boldsymbol{b}))^+; \tag{18}$$

- **Ideal hard magnetic materials are not stable**, since their magnetic polarization is a constant $\boldsymbol{m}_b = M \in \mathbb{R}^n$:

$$\boldsymbol{m}_b(\boldsymbol{b}^+) = M \neq (\boldsymbol{m}_b(\boldsymbol{b}))^+ = M^+. \tag{19}$$

Usual materials and their APBC transformations are listed in Table 1.

$\mathscr{M}$	$\mathscr{M}^+$	$\mathscr{M}^-$
Air	Air (stable)	
Anhysteretic steel	Anhysteretic steel (stable)	
Electric conductor (phase φ)	Electric conductor (phase $\varphi + 180°$)	
PM oriented in θ_m direction	PM oriented in $\theta_m + \theta_{\max} + 180°$ direction	PM oriented in $\theta_m - \theta_{\max} + 180°$ direction

Table 1: Examples of material transformations with APBC (Source: Authors' own work).

The stability concept can be extended to unordered sets of materials.

Definition 3.8 (Stability of a material set)**.** *A material set $\{\mathscr{M}_i\}_{i\in[\![1,n_m]\!]}$ is $\square^+$-stable when $\{\mathscr{M}_i^+\}$, also denoted as $\{\mathscr{M}_i\}^+$, contains the same materials as $\{\mathscr{M}_i\}$.*

Again, $\square^+$ and $\square^-$ stabilities are equivalent, we therefore refer to the stability of $\{\mathscr{M}_i\}$ without specifying the transformation. While a set containing stable materials is obviously stable, other stability cases exist. For instance, a set of two electrical conductors with opposite signs $\{A^+, A^-\}$ is also stable since $\{A^+, A^-\}^+ = \{A^-, A^+\}$ contains the same materials (their order does not matter). To express the filtered density $\tilde{\rho}$ as a linear combination of the candidate materials, the chosen set of candidate materials should be stable. The following subsection shows the converse of this condition by explicitly constructing $\tilde{\rho}$ from a stable material set.

3.4 Transformation of density

In the general case, the application of $\square^+$ to an ordered list of materials $(\mathscr{M}_i)$ from a stable set of materials $\{\mathscr{M}_i\}$ can modify the order of its elements. Using the formalism detailed in Section 2, where $\mathscr{D}$ denotes a convex polytope with n_m vertices, the combination of $\mathscr{D}$ and $(\mathscr{M}_i)$ forms an *interpolation space* $\mathscr{E} = (\mathscr{D}, (\mathscr{M}_i))$ that indicates the placement of each material $\mathscr{M}_i$ on the vertices of $\mathscr{D}$.

Proposition 3.9 (Permutation of the materials)**.** *If $\{\mathscr{M}_i\}$ is stable, then $\mathscr{E}^+ = (\mathscr{D}, (\mathscr{M}_i)^+)$ corresponds to a material placement on $\mathscr{D}$ which has undergone a* ***permutation*** *Π^+:*

$$\forall i \in [\![1, n_m]\!], \quad \{\mathscr{M}_i\}^+ = \{\mathscr{M}_i\} \;\Rightarrow\; \exists \Pi^+, (\mathscr{M}_i)^+ = (\mathscr{M}_{\Pi^+(i)}). \tag{20}$$

Proof. The two lists $(\mathscr{M}_i)$ and $(\mathscr{M}_i)^+$ contain the same elements due to the stability of $\{\mathscr{M}_i\}$. The orderings of their elements may differ, and the bijection between them defines Π^+. ■

Π^+ is also unique if $(\mathscr{M}_i)$ contains no duplicate. Let us denote $\kappa_{\mathscr{E}}(\boldsymbol{\rho})$ a material property interpolated on $\mathscr{E} = (\mathscr{D}, (\mathscr{M}_i))$, with $\{\mathscr{M}_i\}$ a stable material set. Recalling (5), the general expression of an interpolated material property reads

$$\forall \boldsymbol{\rho} \in \mathscr{D}, \forall u, \qquad \kappa_{\mathscr{E}}(\boldsymbol{\rho}, u) = \sum_{i \in [\![1, n_m]\!]} P(\omega_i(\boldsymbol{\rho})) \cdot \kappa_i(u), \tag{21}$$

where u is a physical field, P is a penalty function, ω_i is the shape function associated with the vertex i of $\mathscr{D}$, and κ_i is the property associated with the material $\mathscr{M}_i$. Let $\mathscr{E}^+ = (\mathscr{D}, (\mathscr{M}_i)^+) = (\mathscr{D}, (\mathscr{M}_{\Pi^+(i)}))$. Applying $\square^+$ to $\kappa_{\mathscr{E}}$, we obtain by linearity:

$$\forall \boldsymbol{\rho} \in \mathscr{D}, \forall u, \quad \kappa^+_{\mathscr{E}}(\boldsymbol{\rho}, u) = \sum_{i \in [\![1, n_m]\!]} P(\omega_i(\boldsymbol{\rho})) \kappa^+_i(u) = \sum_{i \in [\![1, n_m]\!]} P(\omega_i(\boldsymbol{\rho})) \kappa_{\Pi^+(i)}(u), \tag{22}$$

or, written differently:

$$\forall \boldsymbol{\rho} \in \mathscr{D}, \forall u, \qquad \kappa^+_{\mathscr{E}}(\boldsymbol{\rho}, u) = \kappa_{\mathscr{E}^+}(\boldsymbol{\rho}, u). \tag{23}$$

In other words, for the same $\boldsymbol{\rho}$ value, the transformed material properties can be expressed naturally in the transformed interpolation space $\mathscr{E}^+$. However, this is still incompatible with filtering, *i.e.*, a linear combination of variables expressed in the *untransformed* space $\mathscr{E}$. The objective is to perform the inverse operation:

$$\text{for a fixed } \boldsymbol{\rho} \in \mathscr{D}, \text{ find } \boldsymbol{\rho}^+ \in \mathscr{D}, \text{ such that } \quad \kappa_{\mathscr{E}}(\boldsymbol{\rho}^+) = \kappa_{\mathscr{E}^+}(\boldsymbol{\rho}), \tag{24}$$

which is illustrated in Figure 7.

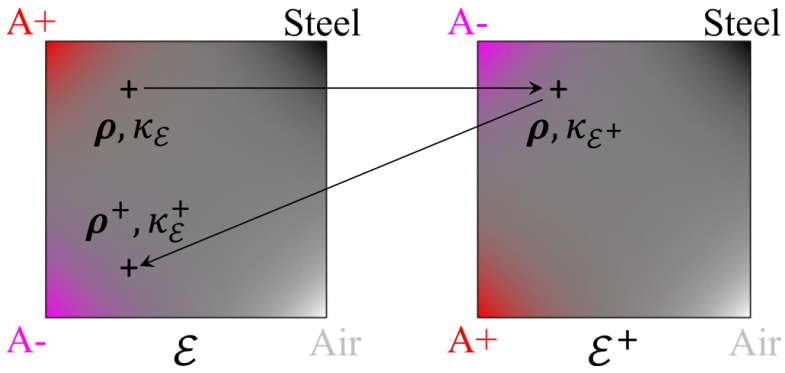

Figure 7: Illustration of the density transformation for a square interpolation domain (Source: Authors' own work).

The existence of Π^+ guarantees the existence of $\boldsymbol{\rho}^+$, which verifies by definition:

$$\forall \boldsymbol{\rho} \in \mathscr{D}, \forall u, \quad \sum_{i \in [\![1, n_m]\!]} P(\omega_i(\boldsymbol{\rho}^+)) \cdot \kappa_i(u) = \sum_{i \in [\![1, n_m]\!]} P(\omega_i(\boldsymbol{\rho})) \cdot \kappa_{\Pi^+(i)}(u), \tag{25}$$

By changing the order of the terms with Π^+ without changing the value of the left sum and taking each term of the sum to be equal, we obtain the following sufficient condition:

$$\forall i \in [\![1, n_m]\!], \qquad \omega_{\Pi^+(i)}(\boldsymbol{\rho}^+) = \omega_i(\boldsymbol{\rho}). \tag{26}$$

We then use the **linear precision** property (3b) fulfilled by the shape functions ω_i, that when applied to $\boldsymbol{\rho}^+$ gives

$$\boldsymbol{\rho}^+ = \sum_{i\in[\![1,n_m]\!]} \omega_i(\boldsymbol{\rho}^+)\boldsymbol{v}_i = \sum_{i\in[\![1,n_m]\!]} \omega_{\Pi^+(i)}(\boldsymbol{\rho}^+)\boldsymbol{v}_{\Pi^+(i)}. \tag{27}$$

We finally obtain the explicit expression of $\boldsymbol{\rho}^+$ by injecting (26) into (27).

Theorem 3.10 (Density transformation)**.** *Let us consider a stable material set $\{\mathscr{M}_i\}_{i\in[\![1,n_m]\!]}$, an interpolation space $\mathscr{E} = (\mathscr{D},(\mathscr{M}_i))$ and a permutation Π^+, such that we have $(\mathscr{M}_i)^+ = (\mathscr{M}_{\Pi^+(i)})$. The transformed density $\boldsymbol{\rho}^+ \in \mathscr{D}$ defining the material interpolated by $\boldsymbol{\rho} \in \mathscr{D}$ reads as*

$$\boldsymbol{\rho}^+ = \sum_{i\in[\![1,n_m]\!]} \omega_i(\boldsymbol{\rho})\boldsymbol{v}_{\Pi^+(i)}. \tag{28}$$

4 Numerical applications

This section illustrates the relevance of the presented filtering methodology on MMTO problems. It also shows the superiority of multi-material approaches compared to standard iron-air optimizations when dealing with a PMSM rotor. In all the numerical experiments, the current density is sinusoidal with an amplitude of $J = 10\,\mathrm{A/mm^2}$, and the magnets are assumed to be ideal with a remanent flux density $B_r = 1\,\mathrm{T}$. The BH curve of the magnetic steel saturates around 2 T and can be found in Cherrière, Vancorsellis, et al., 2023. The initial structure is a homogeneous mixture of all candidate materials, and the filter kernel is a disk with a 2 mm radius. Since the optimization method is deterministic and the problem is not convex, it results in local optima. Additional numerical tests have shown a dependence on the initial situation. For the sake of simplicity, the initialization is a homogeneous mixture of all the materials.

4.1 Reference: bi-material optimizations

The chosen reference is adapted from the BMWi3 machine (Staton and Goss, 2017), and shown in Figure 8a. The associated mesh and boundary conditions, which will be used for all numerical experiments, are drawn in Figure 8b. With a PM volume ratio of 16.42 % of the rotor, the reference design produces a normalized average torque of 2169 Nm/m.

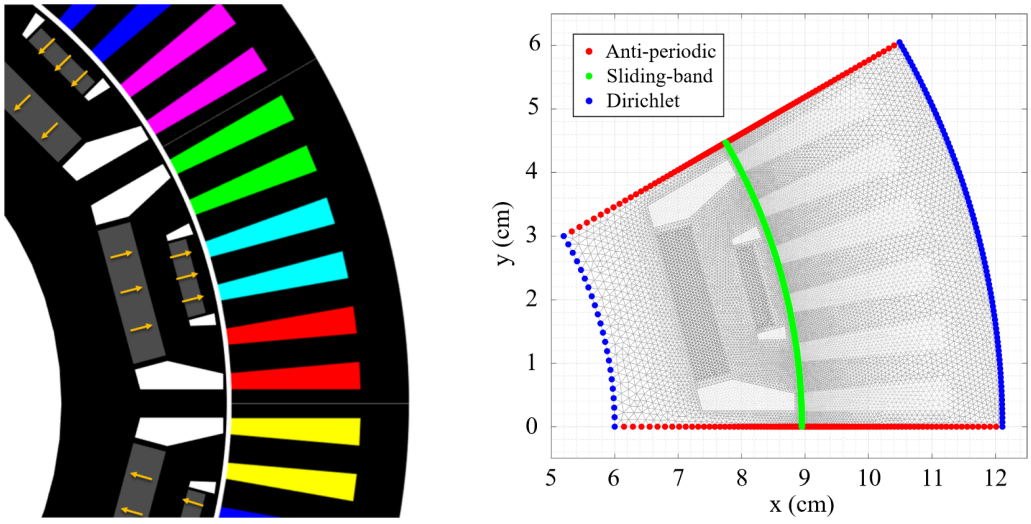

(a) Reference design

(b) Mesh and boundary conditions

Figure 8: Reference design adapted from the BMWi3 PMSM (Staton and Goss, 2017) and associated mesh generated with GMSH (Geuzaine and Remacle, 2009) (Source: Authors' own work).

The reference contains iron on the PMs' sides for mechanical integrity, that are magnetic short-circuited. Since the numerical experiments in this article consider only magnetic performance, we assess our MMTO method with structures obtained with a magnetic-only iron-air TO technique (Cherrière, Hlioui, Laurent, Louf, Ben Ahmed, et al., 2022) to keep a fair comparison. The magnets are fixed and not part of the optimization.

Two different kinds of structures can be obtained. When considering both the motor and generator working points, the optimized rotor shown in Figure 9a is similar to the symmetric reference and produces a torque of 2471 Nm/m. When considering only the motor working point, an asymmetric rotor shown in Figure 9b is obtained and produces a torque of 2638 Nm/m. We keep these torque values as benchmarks for assessing our MMTO approaches in the next subsection.

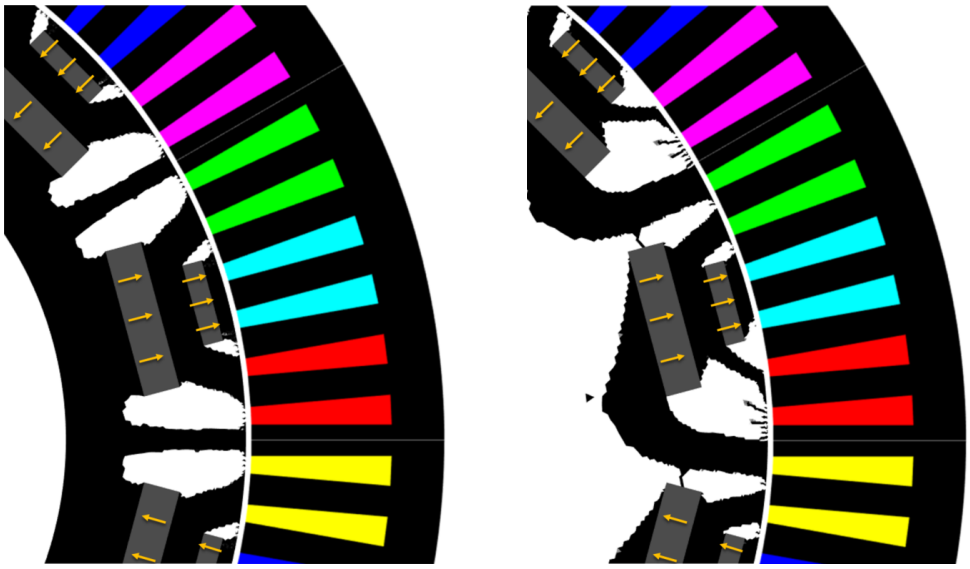

(a) Optimized symmetric rotor (b) Optimized asymmetric rotor

Figure 9: Optimized structure with a iron/air material approach (Source: Authors' own work).

4.2 Multi-material optimizations

In this subsection, we apply MMTO formalism given in Section 2.1 and the optimization algorithm detailed in Section 2.3 to the optimization problem (7) in three different cases:

- without filtering in Section 4.2.1;
- with filtering and cropped kernel on the boundaries in Section 4.2.2;
- with filtering and wrapped kernel using Theorem 3.10 in Section 4.2.3.

The total number of iterations of the optimization algorithm is set to 1000, which represents 20 sub-cycles. The PM volume constraint is set to the reference equal to 16.42 % of the rotor volume. The convergence curves are given with the optimized structures, and the performances are then discussed and compared. In the results that follow, the PMs are drawn in color according to the scale provided in Figure 2a, and the orientation for each magnet is indicated by arrows added for the sake of clarity.

4.2.1 No filtering

First, the algorithm described in Section 2.3 is applied to solve (7) without any filtering. We note on the convergence curve plotted in Figure 10a that the final structure produces 2468 Nm/m, which is less than the torques of both symmetric and asymmetric designs obtained with a iron/air material optimization. In addition, the PM volume is only 14 % instead of the imposed 16.42 %, which shows that the convergence is not reached.

As a result, the final structure drawn in Figure 10b contains many artifacts, such as checkerboards and other microstructures, along with gray materials.

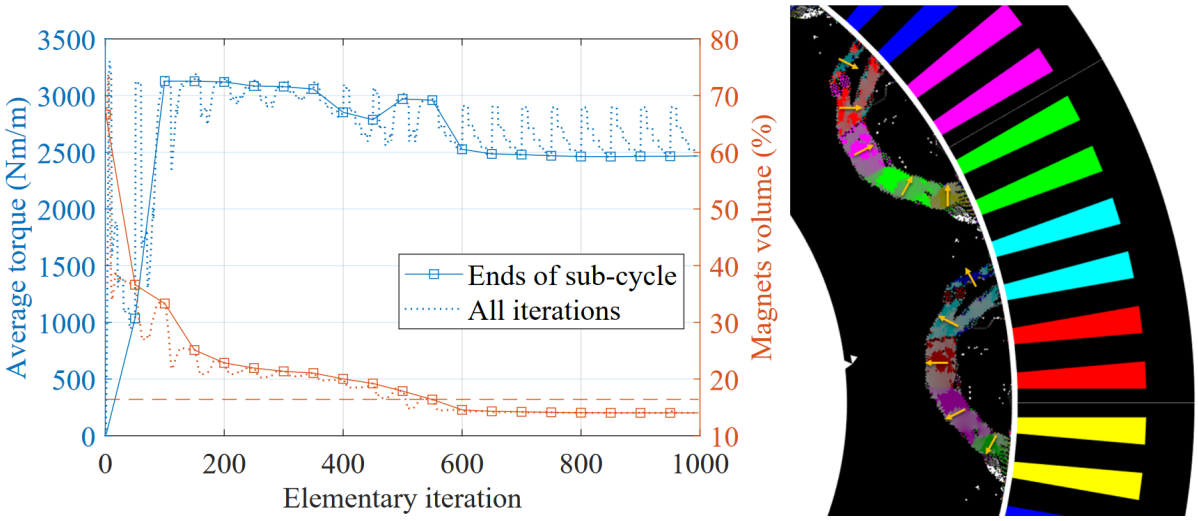

(a) Convergence curves (torque and PM volume)

(b) Final design

Figure 10: MMTO results without filtering (Source: Authors' own work).

This result is not satisfactory and lacks a regularization procedure. Periodic filtering is applied in the following subsections to resolve this issue.

4.2.2 Cropped kernel

In this section, the convolution filtering is cropped at the anti-periodic boundaries. Compared to the results obtained without filtering in Section 4.2.1, the convergence plotted in Figure 11a is improved. Indeed, the average torque reaches 2879 Nm/m, which is significantly higher than what can produce the machines optimized with an iron/air TO. Moreover, the PM volume is 16.28 %, making a relative error on the volume constraint less than 1 %, so this optimized design can be directly compared to the reference.

Most artifacts and intermediate materials have vanished within the resulting structure drawn in Figure 11b, and the magnet zones are clearly defined. However, the boundary of the optimization domain, plotted in the dashed line, seems to disturb the shape of the magnet arc, since it coincides exactly with the material discontinuity circled in yellow.

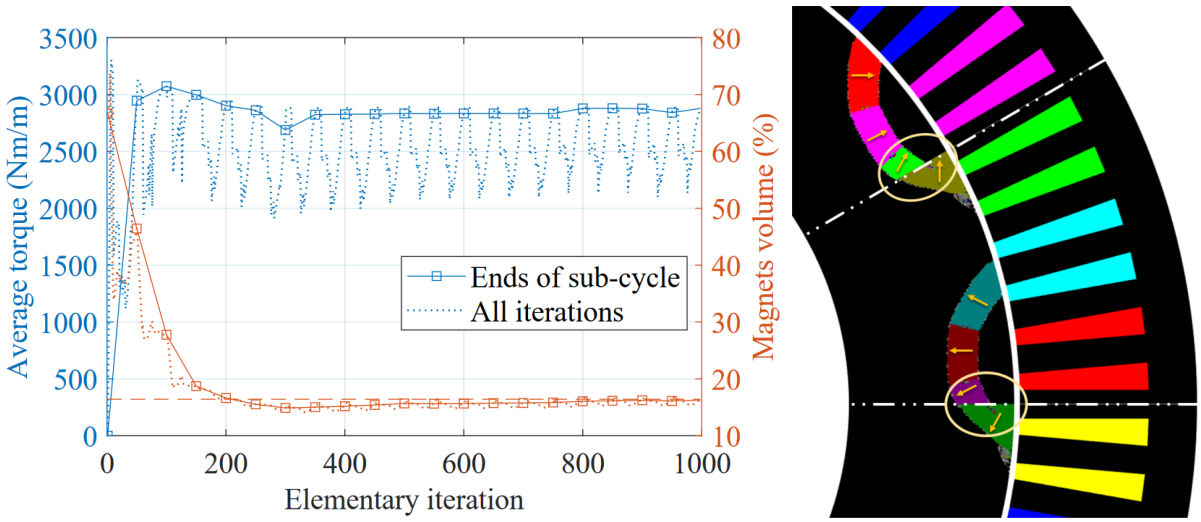

(a) Convergence curves (torque and PM volume) (b) Final design

Figure 11: MMTO results with filtering and a cropped kernel (Source: Authors' own work).

Thus, a cropped convolution kernel introduces a bias in the optimization by neglecting the boundary conditions. The wrapping technique developed in Section 3 should be employed to eliminate this bias.

4.2.3 Wrapped kernel

Compared to a cropped kernel, using a wrapped kernel leads to a similar convergence curve plotted in Figure 12a. The torque reaches 2878 Nm/m, and the PM volume is 16.16 %, almost the same value as the ones obtained with a cropped kernel. However, the wrapping technique removes all artificial boundaries, resulting in the optimized rotor drawn in Figure 12b. This design seems more natural and is what would have been obtained by optimizing the full rotor instead of just a single pole.

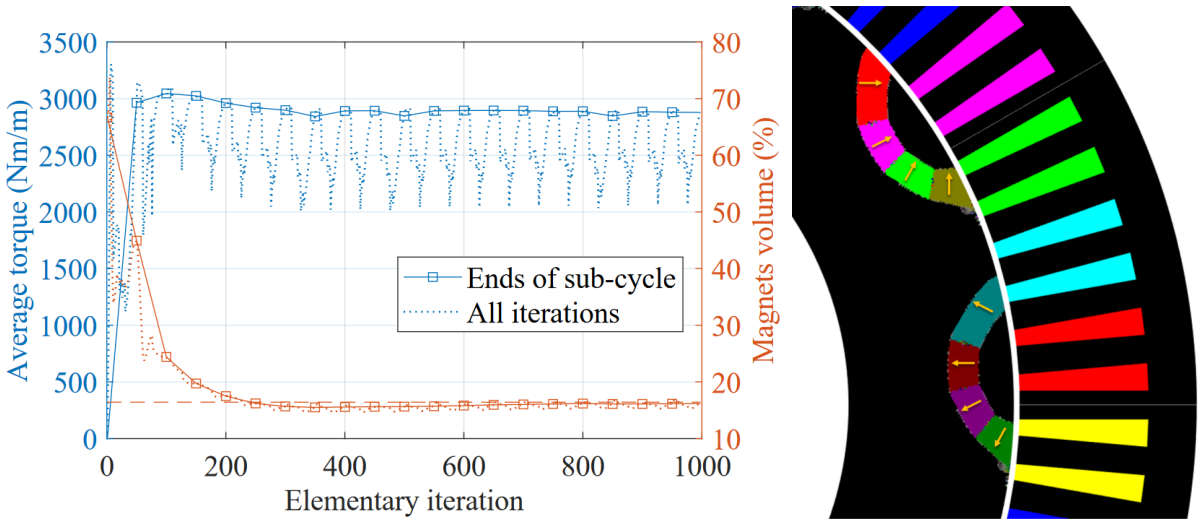

(a) Convergence curves (torque and PM volume) (b) Final design

Figure 12: Optimization results with filtering and a wrapped kernel (Source: Authors' own work).

4.3 Discussion

While filtering appears to improve the optimized structures, some artifacts remain in Figure 11b and Figure 12b, located at some of the boundaries between magnets. This phenomenon can happen since filtering remains a heuristic procedure. In particular, applying any filtering while having a highly penalized interpolation leads to numerical instabilities. Other stabilization procedures can be found in the literature, for example, material projection using a smoothed Heaviside function (Guest, Prévost, and Belytschko, 2004). This work does not cover this technique, which requires further research in order to be generalized to multi-material approaches using shape functions.

Apart from this phenomenon, the third column of Table 2 shows the clear superiority of the designs obtained with MMTO approaches over the iron/air TO with fixed PM. The first two columns also exhibit better convergence when using filtering, which leads to higher torques and helps to satisfy the PM volume constraint. Note that even if the torque obtained using a wrapped kernel is slightly lower than the one obtained with a cropped kernel, the torque/PM ratio is slightly higher for the first one. Therefore, we conclude that an MMTO approach making use of a filtering procedure consistent with the boundary condition can produce better designs with less initial information than traditional TO procedures.

Table 2: Performances comparison of the final designs (Source: Authors' own work).

Rotor type	**Average Torque**	**PM volume**	**Torque / PM volume**
Reference	2173 Nm/m	16,42 %	132 Nm/m/%
Symmetric TO (fixed magnets, Sec. 4.1)	2471 Nm/m	16,42 %	150 Nm/m/%
Asymmetric TO (fixed magnets, Sec. 4.1)	2638 Nm/m	16,42 %	160 Nm/m/%
MMTO (no filter, Sec. 4.2.1)	2468 Nm/m	14,04 %	175 Nm/m/%
MMTO (cropped filter, Sec. 4.2.2)	2879 Nm/m	16,28 %	177 Nm/m/%
MMTO (wrapped filter, Sec. 4.2.3)	2878 Nm/m	16,16 %	178 Nm/m/%

The torque ripple plays an important role in the machine design. From Figure 13, one can evaluate the relative torque ripple of the optimized design from Section 4.2.3 to 25 %. Interestingly, this value is lower than the 35 % ripple of the reference machine from Figure 8a, even without considering the torque ripple in the optimization. This value could be further reduced by including the ripple in the optimization and will be addressed in future work.

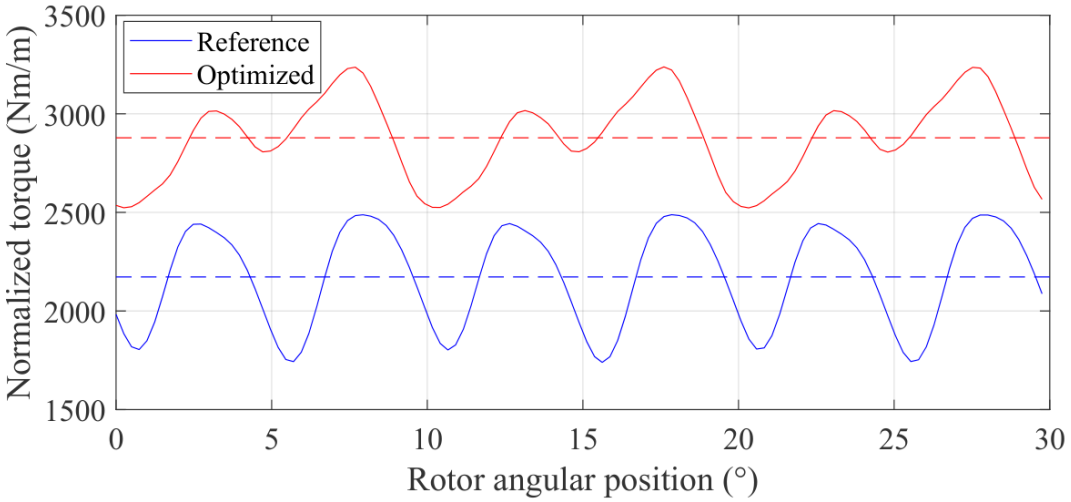

Figure 13: Evolution of the instant torque with the rotor angle (Source: Authors' own work).

5 Conclusion

This work presents a convolution filtering framework, which MMTO problems that include periodic or anti-periodic boundary conditions. Indeed, a naive filtering technique that crops the convolution kernel outside of the simulation domain leads to artificial boundaries on the resulting designs. Consequently, the filtering may introduce a bias in the optimization, as shown on a PMSM rotor. To avoid such an artifact, the present work shows that the set of candidate materials should be carefully chosen: this set must be stable by rotation of any multiple of the angular opening of the simulation domain. Under this assumption, a general wrapping technique that is consistent with the boundary conditions can be applied. The designs optimized with this technique are smoother than the unfiltered results and contain no artificial boundaries, demonstrating the efficiency and unbiasedness of this method. Moreover, a comparison with iron/air TO shows that MMTO approaches are superior for the PMSM rotor test case.

The framework presented here can be extended to continuous approaches, such as Helmholtz-type filtering, suitable to 3D problems (Lazarov and Sigmund, 2010). The boundary conditions on the upper border Γ^+ and the lower one Γ^- should then respect the following constraints

$$(r,\theta) \in \Gamma^+ \Leftrightarrow \boldsymbol{\rho}(r,\theta) = \boldsymbol{\rho}^+(r,\theta-\Delta\theta), \tag{29a}$$

$$(r,\theta) \in \Gamma^- \Leftrightarrow \boldsymbol{\rho}(r,\theta) = \boldsymbol{\rho}^-(r,\theta+\Delta\theta). \tag{29b}$$

This formalism can also be applied in other physics, such as mechanics or thermal. In addition to density, the methodology can be extended to sensitivity filtering, where the material consistency should be applied not to the density field but to its differentiation. Concerning possible other applications, the filtering presented in this paper can be applied to many other MMTO problems currently out of the range of the MMTO literature, such as hybrid-excited machines (Zhu and Cai, 2019).

References

Bendsøe, M. P. and N. Kikuchi (1988). "Generating optimal topologies in structural design using a homogenization method". In: *Computer Methods in Applied Mechanics and Engineering* 71.2, pp. 197–224. DOI: 10.1016/0045-7825(88)90086-2 (cit. on p. 2).

Bendsøe, M. P. (1989). "Optimal shape design as a material distribution problem". In: *Structural Optimization* 1.4, pp. 193–202. DOI: 10.1007/BF01650949 (cit. on p. 2).

Xie, Y. and G. Steven (Dec. 1993). "A simple evolutionary procedure for structural optimization". In: *Computers & Structures* 49.5, pp. 885–896. DOI: 10.1016/0045-7949(93)90035-c (cit. on p. 2).

Wang, M. Y. and S. Zhou (2004). "Phase field: A variational method for structural topology optimization". In: *CMES - Computer Modeling in Engineering and Sciences* 6.6, pp. 547–566. DOI: 10.3970/cmes.2004.006.547 (cit. on p. 2).

Allaire, G., F. Jouve, and A. M. Toader (2004). "Structural optimization using sensitivity analysis and a level-set method". In: *Journal of Computational Physics* 194.1, pp. 363–393. DOI: 10.1016/j.jcp.2003.09.032 (cit. on p. 2).

Amstutz, S. and H. Andrä (Aug. 2006). "A new algorithm for topology optimization using a level-set method". In: *Journal of Computational Physics* 216.2, pp. 573–588. DOI: 10.1016/j.jcp.2005.12.015 (cit. on p. 2).

Liu, J. et al. (May 2018). "Current and future trends in topology optimization for additive manufacturing". In: *Structural and Multidisciplinary Optimization* 57.6, pp. 2457–2483. DOI: 10.1007/s00158-018-1994-3 (cit. on p. 2).

Aage, N. et al. (2017). "Giga-voxel computational morphogenesis for structural design". In: *Nature* 550.7674, pp. 84–86. DOI: 10.1038/nature23911 (cit. on p. 2).

Feppon, F. et al. (Apr. 2021). "Body-fitted topology optimization of 2D and 3D fluid-to-fluid heat exchangers". In: *Computer Methods in Applied Mechanics and Engineering* 376, p. 113638. DOI: 10.1016/j.cma.2020.113638 (cit. on p. 2).

Bruyneel, M. (2011). "SFP-a new parameterization based on shape functions for optimal material selection: Application to conventional composite plies". In: *Structural and Multidisciplinary Optimization* 43.1, pp. 17–27. DOI: 10.1007/s00158-010-0548-0 (cit. on p. 2).

Dyck, D. N. and D. A. Lowther (1996). "Automated design of magnetic devices by optimizing material distribution". In: *IEEE Transactions on Magnetics* 32.3 PART 2, pp. 1188–1192. DOI: 10.1109/20.497456 (cit. on p. 2).

Lee, J., J. H. Seo, and N. Kikuchi (2010). "Topology optimization of switched reluctance motors for the desired torque profile". In: *Structural and Multidisciplinary Optimization* 42.5, pp. 783–796. DOI: 10.1007/s00158-010-0547-1 (cit. on p. 2).

Lucchini, F. et al. (2022). "Topology Optimization for Electromagnetics: A Survey". In: *IEEE Access* 10.August, pp. 98593–98611. DOI: 10.1109/access.2022.3206368 (cit. on p. 2).

Lee, C. and I. Gwun (2022). "Multi - material topology optimization for the PMSMs under the consideration of the MTPA control". In: *Structural and Multidisciplinary Optimization*, pp. 1–11. DOI: 10.1007/s00158-022-03367-x (cit. on pp. 2–3).

Cherrière, T., L. Laurent, et al. (2022). "Multi-material topology optimization using Wachspress interpolations for designing a 3-phase electrical machine stator". In: *Structural and Multidisciplinary Optimization* 65.352. DOI: 10.1007/s00158-022-03460-1 (cit. on pp. 2, 4–5).

Sigmund, O. (Oct. 2001). "Design of multiphysics actuators using topology optimization – Part II: Two-material structures". In: *Computer Methods in Applied Mechanics and Engineering* 190.49-50, pp. 6605–6627. DOI: 10.1016/s0045-7825(01)00252-3 (cit. on p. 2).

Abdelhamid, M. and A. Czekanski (2022). "Revisiting non-convexity in topology optimization of compliance minimization problems". In: *Engineering Computations (Swansea, Wales)* 39.3, pp. 893–915. DOI: 10.1108/EC-01-2021-0052 (cit. on p. 3).

Sigmund, O. and J. Petersson (1998). "Numerical instabilities in topology optimization: A survey on procedures dealing with checkerboards, mesh-dependencies and local minima". In: *Structural Optimization* 16.1, pp. 68–75. DOI: 10.1007/BF01214002 (cit. on pp. 3, 7).

Lazarov, B. S. and O. Sigmund (Dec. 2010). "Filters in topology optimization based on Helmholtz-type differential equations". In: *International Journal for Numerical Methods in Engineering* 86.6, pp. 765–781. DOI: 10.1002/nme.3072 (cit. on pp. 3, 16).

Bourdin, B. (2001). "Filters in topology optimization". In: *International Journal for Numerical Methods in Engineering* 50.9, pp. 2143–2158. DOI: 10.1002/nme.116 (cit. on p. 3).

Clausen, A. and E. Andreassen (2017). "On filter boundary conditions in topology optimization". In: *Structural and Multidisciplinary Optimization* 56.5, pp. 1147–1155. DOI: 10.1007/s00158-017-1709-1 (cit. on p. 3).

Wallin, M. et al. (2020). "Consistent boundary conditions for PDE filter regularization in topology optimization". In: *Structural and Multidisciplinary Optimization* 62.3, pp. 1299–1311. DOI: 10.1007/s00158-020-02556-w (cit. on p. 3).

Kumar, P. and E. Fernández (2021). "A numerical scheme for filter boundary conditions in topology optimization on regular and irregular meshes". In: (cit. on p. 3).

Korman, O. et al. (2022). "On the Use of Topology Optimization for Synchronous Reluctance Machines Design". In: *Energies* 15.10. DOI: 10.3390/en15103719 (cit. on p. 3).

Cherrière, T., S. Hlioui, L. Laurent, F. Louf, H. Ben Ahmed, et al. (2022). "Topology Optimization of Asymmetric PMSM Rotor". In: *2022 International Conference on Electrical Machines (ICEM)*, pp. 469–475. DOI: 10.1109/ICEM51905.2022.9910650 (cit. on pp. 3, 12).

Gauthey, T., M. H. Hassan, et al. (Mar. 2024). "Topology Optimization of the Harmonic Content for Torque Ripple Minimization". In: *IEEE Transactions on Magnetics* 60.3, pp. 1–4. DOI: 10.1109/tmag.2023.3303679 (cit. on p. 3).

Cherrière, T., T. Vancorsellis, et al. (2023). "A Multimaterial Topology Optimization Considering the PM Nonlinearity". In: *IEEE Transactions on Magnetics* 59.5, pp. 1–9. DOI: 10.1109/TMAG.2023.3256003 (cit. on pp. 3, 11).

Gauthey, T., P. Gangl, and M. Hage Hassan (2022). "Multi-Material Topology Optimization with Continuous Magnetization Direction for motors design". In: *2022 International Conference on Electrical Machines (ICEM)*, pp. 483–489. DOI: 10.1109/ICEM51905.2022.9910654 (cit. on p. 3).

Cherrière, T., S. Hlioui, L. Laurent, F. Louf, H. B. Ahmed, et al. (2024). "Effects of Filtering and Current-Angle Adjustment on the Multi-Material Topology Optimization of a Three-Phase Stator". In: *IEEE Transactions on Magnetics* 60.3, pp. 1–4. DOI: 10.1109/TMAG.2023.3317700 (cit. on pp. 3, 5).

Warren, J. et al. (Dec. 2006). "Barycentric coordinates for convex sets". In: *Advances in Computational Mathematics* 27.3, pp. 319–338. DOI: 10.1007/s10444-005-9008-6 (cit. on p. 4).

Wachspress, E. L. (1975). *A Finite Element Rational Basis*. Vol. 114. Mathematics in Science and Engineering. Academic Press, Inc. DOI: 10.1016/s0076-5392(09)60113-2 (cit. on p. 4).

Cherrière, T. and L. Laurent (2022). *Wachspress2D3D, v1.0.0*. Code Matlab. DOI: 10.5281/zenodo.6630215 (cit. on p. 4).

Bendsøe, M. P. and O. Sigmund (Nov. 1999). "Material interpolation schemes in topology optimization". In: *Archive of Applied Mechanics (Ingenieur Archiv)* 69.9-10, pp. 635–654. DOI: 10.1007/s004190050248 (cit. on p. 4).

Stolpe, M. and K. Svanberg (2001). "An alternative interpolation scheme for minimum compliance topology optimization". In: *Structural and Multidisciplinary Optimization* 22.2, pp. 116–124. DOI: 10.1007/s001580100129 (cit. on p. 4).

Arkkio, A. (1987). "Analysis of Induction Motors Based on the Numerical Solution of the Magnetic Field and Circuit Equations." PhD thesis. Helsinki University of Technology (cit. on p. 5).

Nocedal, J. and S. J. Wright (2006). *Numerical optimization*. Springer New York, NY, pp. 1–664. DOI: 10.1007/978-0-387-40065-5 (cit. on p. 5).

Cea, J. (1986). "Conception optimale ou identification de formes, calcul rapide de la dérivée directionnelle de la fonction coût". In: *ESAIM: Mathematical Modelling and Numerical Analysis* 20.3, pp. 371–402. DOI: 10.1051/m2an/1986200303711 (cit. on p. 5).

Staton, D. and J. Goss (2017). "Open Source Electric Motor Models for Commercial EV Hybrid Traction Motors". In: *CWIEME*. Berlin (cit. on p. 11).

Geuzaine, C. and J. Remacle (2009). "Gmsh: A 3-D finite element mesh generator with built-in pre- and post-processing facilities". In: *International Journal for Numerical Methods in Engineering* 79.May, pp. 1309–1331. DOI: 10.1002/nme.2579 (cit. on p. 11).

Guest, J. K., J. H. Prévost, and T. Belytschko (Aug. 2004). "Achieving minimum length scale in topology optimization using nodal design variables and projection functions". In: *International Journal for Numerical Methods in Engineering* 61.2, pp. 238–254. DOI: 10.1002/nme.1064 (cit. on p. 15).

Zhu, Z. Q. and S. Cai (2019). "Hybrid Excited Permanent Magnet Machines for Electric and Hybrid Electric Vehicles". In: *CES Transactions on Electrical Machines and Systems* 3.3, pp. 233–247. DOI: 10.30941/CESTEMS.2019.00032 (cit. on p. 16).